JOURNAL OF MATERIALS SCIENCE 29 (1994) 1169–1173

Identification of surface carbides and spinels in welded austenitic stainless steels

M. AHMAD, K. A. SHOAIB, M. A. SHAIKH, J. I. AKHTAR
Radiation Damage Group, Nuclear Physics Division, Pakistan Institute of Nuclear Science and Technology, P.O. Nilore, Islamabad, Pakistan

Welding of stainless steels has been shown to cause localized changes in the microstructure and chemical composition which could have adverse implications for the mechanical and corrosion properties of the material. The application of several electron-optical techniques, such as transmission and scanning electron microscopies (TEM, SEM) and electron and Auger microprobe analysis (AEM), for the identification of different phases has been illustrated by the investigation of segregation effects in welded steels of AISI types 304, 304L, 316 and 316L. Considerable enhancement of chromium and carbon has been observed in certain well-defined zones on the parent metal and on the weld beads. Enhancement of oxygen was also observed at some of the points in these areas. The localized change in surface composition, particularly in the parent metal is attributed to the formation of the carbide $M_{23}C_6$ and the spinel $FeCr_2O_4$. The results were confirmed by the determination of the composition of the segregation zone, as well as the lattice parameter of some of the particles, with TEM, SEM and AEM.

1. Introduction

AISI-304 is a general purpose corrosion-resistant austenitic stainless steel commonly used in industrial fabrication. Stainless steel of type AISI-316 has a much higher corrosion resistance and creep strength and has specialized, but extensive, uses, such as those in chemical plants, as superheater piping and tube material in steam generating plants, as a structural material and a cladding alloy in conventional and advanced nuclear reactors.

Austenitic stainless steels have been widely used as a superheater and reheater tube material in fossil fuel power plants. Because the interior metal surface is exposed to high-temperature steam, the steam oxidation of these steels has become the major corrosion problem for these materials. The oxide scales generated in steam exhibit a duplex layer structure, the outer layer being composed mainly of Fe_3O_4 and the inner layer of $(FeCr)_3O_4$ spinels [1]. In the case of steels, spinel phases often appear in greater abundance upon oxidation in air [2].

Another common problem resulting from the exposure of stainless steels to high temperatures is the formation of carbides and intermetallic phases. The major phases observed in type 316 stainless steel include the carbides $M_{23}C_6$, M_6C, M_7C_3 and the intermetallics σ, χ and η [3, 4]. The welding technique, which is used in the construction of modern structures, involves melting and solidification of the material. This could cause changes in the microstructure and chemical composition of the material which can adversely affect the mechanical and corrosion properties.

In work done previously on the welded [4–8] and post-weld heat-treated [6, 7, 9] samples 304 and 316, the weld zone has been studied which showed enhancement of certain elements, but results of surface segregation on the matrix have so far not been reported. The present paper describes experimental results of the investigation of welded austenitic stainless steels showing distinct zones of segregation on the parent metal away from the welded area. The powerful role that can be played by the combined application of a number of electron optical techniques in the characterization of the microstructure of materials is highlighted.

2. Experimental procedure

The materials investigated are the austenitic stainless steels of the AISI type 304, 304L, 316 and 316L obtained from commercial sources. Table I gives the nominal composition of the four alloys. Steels 304L and 316L have lower carbon content than 304 and 316. The samples of steels 304, 304L and 316 were in the form of a disc of thickness 3 mm and of diameter 20 mm, while the samples of steel 316L were in the form of rectangular strips, approximately 15 mm $\times$ 25 mm $\times$ 0.68 mm in size. Rectangular samples of steel 304L and 316L of the size 20 mm $\times$ 20 mm and thickness 3 mm were also investigated. A diametrical V-groove of 2 mm width and the same depth was cut in all the 3 mm thick specimens.

The test welds were produced using a tungsten inert gas welding technique with the shielding gas being argon flowing at a rate of 5–10 l min^{-1}. The multipass

0022–2461

welds were produced by employing the method of forward welding in which the electrode was held at an angle of 45° and was given side to side motion in a weaving manner. The filler metal was derived from the parent metal in the form of 1–2 mm wide strips. The tungsten electrode had a diameter of 1.0–1.6 mm and the weld travel speed ranged from 0.5–1.0 mm s^{-1}. The welding current was about 30 and 12 A for the thick and thin samples, respectively, which was reduced to 5 and 2.5 A towards the end of the welding sequence, in order to account for the heat accumulation. The welded samples were etched at 70 °C for 4 min in a 1:1 solution of conc. HCl in water in order to reveal surface segregation. Different etching times were tried and after every etching the sample was examined in a scanning electron microscope. An etching time of 4 min was chosen, because it revealed the segregation zone without losing any information. Carbon extraction replicas were also prepared from the segregation area, which were stripped electrolytically in a solution of 20% HCl in ethanol. The samples were examined with JEOL JSM-35CF scanning electron microscope using an electron beam of 25 kV. Microprobe analysis was done using an automated energy dispersive system (Link 860-2) and JEOL wavelength dispersive spectrometer DDS attached to the microscope. A transmission electron microscope JEM 2000 FX, with an X-ray microanalyser TN 5500 attached, was used for the determination of the composition and lattice parameter of the extracted particles. A scanning electron microscope (Philips SEM 505) with an energy dispersive windowless detector attached, as well as an Auger electron microprobe VG MICROLAB 310-D, was used to confirm the presence of light elements carbon and oxygen.

3. Results and discussion

Visual inspection of the etched samples showed large black zones, about 1 mm wide, in some parts of the parent metal in all the samples of stainless steels. These zones, for the disc and rectangular specimens, are illustrated in Fig. 1. The outstanding feature of these zones was their geometry. In circular specimens the zones were towards the end of the welding sequence and were a circular segment around the last weld bead, whereas in the rectangular specimens the zone was a straight line parallel to the welded zone which grew darker towards the end of the welding sequence. Low-magnification examination in an optical stereomicroscope also showed scattered dark spots on the weld metal beads, their density generally increasing towards the last bead.

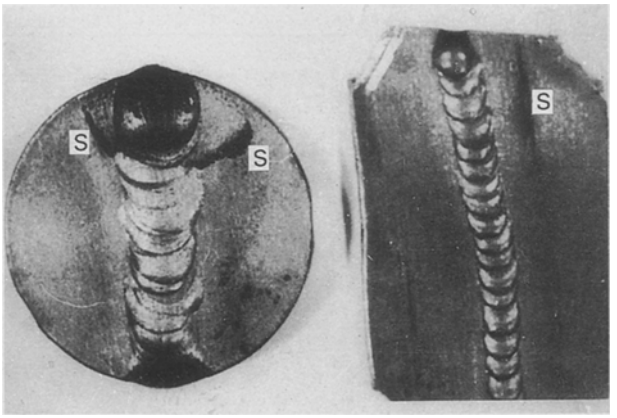

Figure 1 Low-magnification photograph of welded areas and black zones indicated by S.

X-ray microanalysis measurements have been made at particular spots and areas representing (a) the heat-affected zones; (b) the last weld bead; (c) overlapping boundaries of the last two beads; and (d) the parent metal. The results show that average composition of the heat-affected zones and of the weld beads was generally the same as that in the parent metal. However, in isolated spots, considerable increase was observed in the chromium content. In the heat-affected zones these spots are seen near the black areas while the density of such spots on weld beads increases towards the last weld bead. The results are summarized in Table II in terms of Cr:Fe ratios for the parent metal and for the selected spots with high segregation in the welded specimens.

The parent matrix in all the four steels exhibited marked enhancement of chromium in the black zones, hereafter referred to as segregation zones, the maximum content being nearly 60% in 304 steel. Fig. 2 is a micrograph of such an area and shows the line profiles of chromium and iron with the line scan done along the central straight line. The segregates on parent metal can be seen to be in the form of thin flakes. It is evident that chromium increases considerably in the segregation zone, while iron decreases correspondingly. A similar effect can also be seen in a narrow region of the heat-affected zone adjacent to the weld bead. The superficial nature of the zone is revealed in Fig. 3, which gives the Cr:Fe and Ni:Fe ratios, and the carbon profile, determined along the central straight line, in a selected area within the weld beads of 304 samples cut in cross-section. The depth of the surface segregates can be seen to be about 20 μm.

Similar results are obtained for other steel samples for the segregation areas on the parent metal. However, the magnitude of Cr:Fe ratio differs in all the

TABLE I Composition of the investigated stainless steels (wt %)

Sample	Cr	Ni	Mn	Mo	C	N	Si	P	S	Fe
304	19.0	9.3	2.0	–	0.08	0.03	1.0	0.005	0.03	Bal.
304L	19.0	10.0	2.0	–	0.03	0.03	1.0	0.005	0.03	Bal.
316	17.6	11.6	1.3	2.7	0.06	0.03	0.5	0.002	0.01	Bal.
316L	17.0	12.0	2.0	2.5	0.03	0.03	1.0	0.005	0.03	Bal.

TABLE II Cr:Fe ratio for the steels investigated. The values, other than those for parent metal, represent only those spots or areas with high segregation

Sample	Parent metal (average)	Weld, last bead	Heat-affected zone	Overlapping boundaries of beads	Base metal segregation
304	0.28	1.37	1.69	1.55	1.96
304L	0.28	0.33	0.44	0.34	1.22
316	0.27	0.29	0.35	0.59	0.65
316L	0.26	1.52	0.79	2.11	0.93

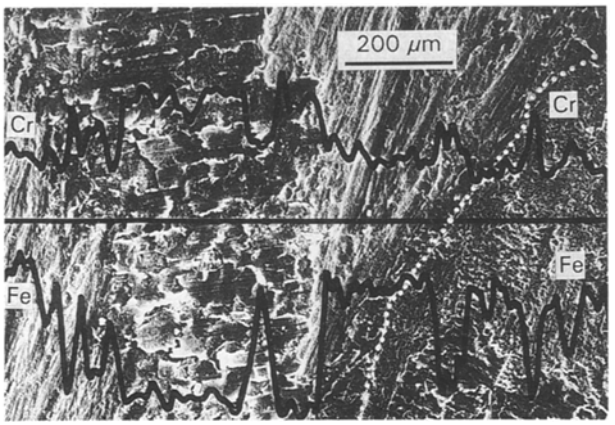

Figure 2 Line scan of a segregation area on the parent metal in welded 304 steel, showing the enhancement of chromium and a corresponding decrease in iron content. The white dashed line indicates the edge of the weld bead, which is to the right.

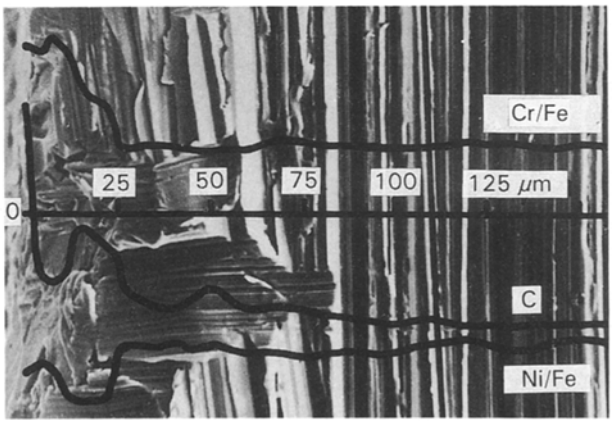

Figure 3 Profiles showing Cr:Fe, Ni:Fe ratios and the carbon content in a cross-sectional slice inside the weld bead showing enhancement in chromium and carbon near the surface (at 0 μm) of the bead.

samples. An increase in Ni:Fe ratio, accompanied by increase in molybdenum content, has also been observed in such segregation areas of 316 and 316L steels. An increase in the Cr:Fe ratio is sometimes also observed at the overlapping of two beads which is prominent in the case of 316L steel (Table II) where segregation is observed over a wider area. Enhancement of chromium in the segregation area would lead to its depletion in the areas (of sample) in the vicinity. Simple calculations show that if the additional chromium in the segregation zone is assumed to come from the volume of the sample underneath this zone, it would result in a reduction of 0.5% in the chromium content. This is within the experimental error and is the probable reason why the depletion could not be detected by normal X-ray microanalysis.

Analysis of extracted replicas from the segregation zones was done using a scanning transmission electron microscope with X-ray microanalysis attachment. One such spectrum from a precipitate showing the chromium and iron contents is given in Fig. 4. Although the contents of the iron and chromium for different precipitates, the Cr:Fe ratio in most cases is 2:1. A small amount of nickel was also observed in a few precipitates. The observed composition of the precipitates suggests the formation of $M_{23}C_6$, which is usually found in heat-treated stainless steels, and a Cr:Fe ratio of about 2:1 is often described as the "signature" of the carbide in energy dispersive analysis where the carbon content cannot be determined.

Fig. 5 shows the ED spectrum from the segregation zone of a 304 steel sample obtained using SEM with a windowless detector which confirms the enhancement of chromium, carbon and oxygen. Wavelength dispersive measurement, done for the light elements revealed a considerable increase of carbon at segregation zones in all the specimens with occasional detection of oxygen at some points. Analysis was also done at the normal matrix and the segregation zones using the Auger electron microprobe, and carbon and

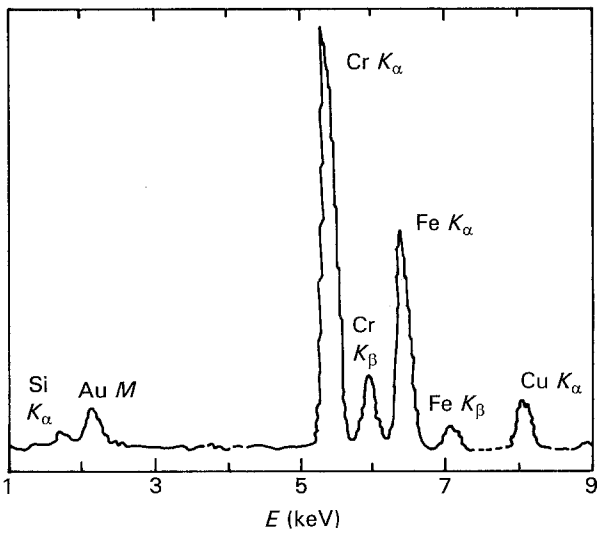

Figure 4 X-ray spectrum obtained with the TEM with energy dispersive microanalyser, showing the enhancement of chromium in an extraction replica from the segregation zone. The copper peak is from the grid and that of gold from the surface coating.

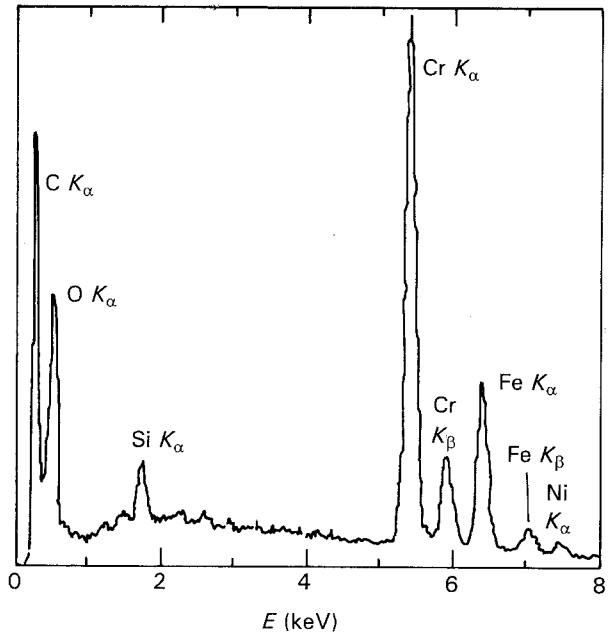

Figure 5 X-ray spectrum obtained with the SEM with a windowless ED detector showing the enhancement of carbon, oxygen and chromium in selected area on the parent metal.

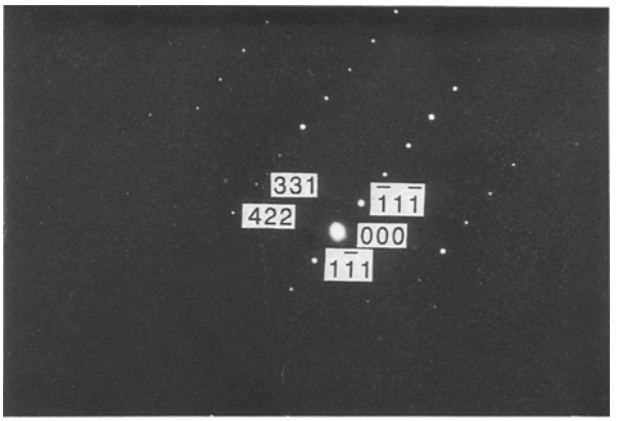

Figure 6 A diffraction pattern used for the determination of the lattice parameter of the thin particles stripped from surface segregation on a welded 304 steel specimen. The direction is $[2\,\bar{1}\,\bar{3}]$.

oxygen were detected in all the areas. Concentration profiles were taken with increasing time of surface sputtering by the argon ions inside the instrument. After sputtering for 300 s (removing a surface layer of 50 nm), the carbon content became very low in the normal matrix. On the other hand, the concentration of carbon in the segregation zone, although decreased to a certain extent, remained very high. The chromium signal increased throughout the depth profile and the concentrations of chromium and carbon were very high and that of iron very low in the segregation area, compared to that in the matrix. The simultaneous enhancement of chromium and carbon, as indicated by both Auger and electron probe microanalysis, characterizes the segregation zone to be predominantly composed of carbides [10].

Diffraction patterns of extraction replicas were taken in the TEM for the determination of the crystal structure and lattice parameter for the possible coexistence of oxides along with the carbides. The diffraction pattern (Fig. 6) could, however, be obtained from only very thin electron-transparent particles, which formed a very small fraction of the extracted segregates. The lattice parameter, a_0, was calculated from the diffraction patterns which indexed as fcc. The parameter a_0 for these particles was found to be 0.82–0.83 nm which corresponds to that of the spinel $FeCr_2O_4$. On the other hand, the lattice parameter of $Cr_{23}C_6$, which also has a complex cubic structure, is 1.060 nm. It could thus be said that the composition of the small number of electron-transparent surface segregates whose lattice parameter could be measured, is $FeCr_2O_4$. Auger analysis and windowless ED detection had already indicated the presence, though not very widespread, of oxygen. The formation of the spinel phase could be attributed to oxygen impurity in the commercial grade argon used as shielding gas, which may have caused some oxidation of the specimens.

Diffraction patterns could not be obtained from thick particles in the extraction replica. However, as discussed before, the Cr:Fe ratio and the considerable amount of carbon detected by various techniques convincingly demonstrates the presence of $M_{23}C_6$. It is, therefore, most likely that the majority of segregation zones and the thick precipitates consist of $M_{23}C_6$. The segregation of chromium in the form of carbides was also confirmed during the experiments conducted on rod-shaped specimens whose one end was heated by TIG welding to the molten state and the analysis was done on the interior (where no oxygen is available) in the form of slices cut at various distances from the molten zone [11]. The formation of $M_{23}C_6$ carbides is well known in these steels and is explained on the basis of the fast diffusion of chromium and interstitial carbon rejected from the austenitic matrix below 900 °C. Varying amounts of other elements such as nickel and molybdenum can replace chromium in the lattice of $M_{23}C_6$ [12].

The formation of well-defined zones of segregation area around the last weld bead could be explained on the basis of a time–temperature–precipitation (TTP) curve [3] for $M_{23}C_6$ in stainless steel. Such diagrams are modified by composition and thermomechanical pre-treatment and could be displaced in terms of time–temperature coordinates, but they essentially retain the same features. The TTP curves of steels studied in the present work are likely to be similar. In both the circular and rectangular specimens, the segregated zone appears near the end of the welding sequence. From the TTP curve it is clear that precipitation of $M_{23}C_6$ results if the sample remains at a particular temperature for a certain period of time. The area near the end of the welding sequence is likely to fulfil the requirements of both time and temperature. Though the temperature at other points may be high enough for precipitation, the time may not be sufficient. A similar effect was observed in the experiment on end-welded rod experiments where a maximum concentration of $M_{23}C_6$ was found at a certain distance away from the molten end. The occurrence of

a segregated zone in the form of a circular segment in circular samples and a line parallel to beads in rectangular samples is expected due to the difference in the shape of the isotherms on account of sample geometry.

4. Conclusions

Welding of austenitic stainless steels 304 and 316 causes the formation of certain distinct zones rich in chromium which are composed of carbide $M_{23}C_6$ and spinel $FeCr_2O_4$. Complementary use of different electron-optical techniques such as scanning electron microscopy (with ED, WD and windowless detection systems), transmission electron microscopy (with ED system) and Auger electron microanalysis, has been shown to be essential for differentiation between carbides and spinels.

Acknowledgements

The authors gratefully acknowledge VG Scientific Limited, UK, for the analysis of the specimens on Auger Electron Microprobe. They are also grateful to other members of Radiation Damage Group for their technical help.

References

1. N. OTSUKA, Y. SHIDA and H. FUJIKAWA, *Oxid. Metals* **32** (1989) 13.
2. O. KUBASCHEWSKI and B. E. HOPKINS, "Oxidation of Metals and Alloys", 2nd Edn (Butterworths, London, 1962) p. 133.
3. B. WEISS and R. STICKLER, *Metall. Trans.* **3** (1972) 851.
4. A. A. TAVASSOLI, A. BISSON and P. SOULAT, *Metal Sci.* **8** (1984) 345.
5. T. TAKALO, N. SUUTALA and T. MOISIO, *Metall. Trans.* **10A** (1979) 1173.
6. G. F. SLATTERY and P. O. RIORDAN, *Metallography* **13** (1980) 59.
7. J. FOULDS and J. MOTEFF, *Metall. Trans.* **13A** (1983) 173.
8. J. C. LIPPOLD and W. F. SAVAGE, *Weld. J.* **61** (1982) 388s.
9. V. S. RAGUNATHAN, V. SEETHARAMAN, S. VENKADESAN and P. RODRIGUEZ, *Metall. Trans.* **10A** (1979) 1683.
10. J. K. L. LAI, D. J. CHASTELL and P. E. J. FLEWITT, *Mater. Sci. Eng.* **49** (1981) 19.
11. A. WAHEED, MSc nuclear engineering thesis, Quaid-i-Azam University, Islamabad, Pakistan (1986).
12. D. V. EDMONDS and R. W. K. HONEYCOMBE, "Precipitation Processes in Solids", edited by K. C. Russell and H. I. Aaronson (Metallurgical Society of AIME, Warrendale, PA, 1978) p. 121.

Received 24 March 1992
and accepted 9 September 1993